

Effect of Three Different Electrolyte Additives on Corrosion Resistance of Micro-arc Oxidation Coating of NiTi Alloy in Simulated Body Fluid

Yao Yao, Wenlan Cai, Zhenxia Wang*, Naiming Lin, Linhai Tian, Lin Qin, Yucheng Wu*

Institute of New Carbon Materials, Taiyuan University of Technology, 030024

*E-mail: wangzhenxia@tyut.edu.cn; wyc@tyut.edu.cn

Received: 6 July 2020 / Accepted: 7 September 2020 / Published: 31 October 2020

In this paper, a micro-arc oxidation (MAO) coating was formed on NiTi alloy in a 0.2 mol/L NaAlO₂ base electrolyte with three additives of 0.03 mol/L NaOH, 0.03 mol/L NaH₂PO₂ and 0.03 mol/L Na₃PO₄, respectively. The influence of different additives on the surface morphology and corrosion resistance of the MAO coatings was systematically investigated. The result revealed that a relatively flat MAO ceramic coating with a typical MAO porous morphology was presented in the electrolyte with NaH₂PO₂. The coating showed the best corrosion resistance which was verified by the smallest corrosion current density after polarization test, indicating that NaH₂PO₂ was an ideal additive. On the base of the above results, MAO-NaH₂PO₂ coating was mainly studied. The section morphology indicated that the MAO-NaH₂PO₂ coating was composed of the dense inner layer and loose outer layer, with a thickness of 5.4 μm. XRD showed that the MAO-NaH₂PO₂ coating was mainly composed of Al₂O₃. It was also proved that the wear resistance of the MAO-NaH₂PO₂ coating had been improved.

Keywords: NiTi alloy; micro-arc oxidation; corrosion resistance; wear resistance

1. INTRODUCTION

Equiatomic nickel-titanium (NiTi) alloy is very attractive for biomedical applications due to its shape memory effect, good biocompatibility and superelasticity[1, 2]. Biocompatibility and corrosion resistance are the most important factors of NiTi alloy as implant materials. The toxicity caused by the release of nickel ions is the primary cause of the decrease in the biocompatibility of NiTi implants. Nickel is essential to the biological function of the human body in terms of nutrition, since it is necessary for the biosynthesis of the hydrogenase, carbon monoxide dehydrogenase. The nickel demands of human beings and animals amount to less than 500 mg/kg, and possibly even lower [3, 4]. But the NiTi alloy as an implant can release a higher level of nickel, which can cause severe rashes,

toxicity and carcinogenic symptoms[5]. On the other hand, NiTi alloys will be easy to be corroded and worn after implantation, which will further aggravate the release of nickel ions. The toxicity and biological activity of NiTi alloy depend on its surface state. To solve this problem, the coatings with good wear resistance, corrosion resistance and biological activity are made on the surface of NiTi alloy.

There are several useful NiTi coating techniques, such as anodizing[6], electrophoresis and electrodeposition[7-9], laser surface modification[10-12], ion implantation[13, 14], magnetron sputtering[15, 16] and micro-arc oxidation coating(MAO)[17, 18]. Although all the introduced methods are reliable in the coating, MAO is considered to be a promising process due to its simplicity, low cost and friendly to environment. It is a new type of liquid phase surface modification technology developed based on anodic oxidation technology. And, it is a new technology that directly grows ceramic layers on the surface of valve metals such as aluminium, magnesium, titanium and their alloys [19, 20].

Among many factors that affect the structure and properties of micro-arc oxidation coating, electrolyte composition is important factor. It affects not only the growth process of ceramics layer, but also the properties of the ceramic coatings. The electrolytes used in micro-arc oxidation treatment can be divided into two categories: acidic electrolytes and alkaline electrolytes. Acidic electrolyte can usually cause environment pollution and strong corrosive, so it is seldom used. The weak alkaline electrolyte has become the main research object in recent years, mainly including phosphate system, silicate system and aluminate system according to the main coating-forming elements. Wang et al.[21-23] found that different electrolytes (H_3PO_4 , H_2SO_4 and NaAlO_2) represent different barrier layer formation mechanisms in their works. In this paper, the aluminate system is proposed because of its better wear resistance and coating adhesion compared with the other two systems[24]. In the meanwhile, the coating prepared in an electrolyte formed by the addition of three different additives to the NaAlO_2 base solution was studied. The different additives will directly affect the generation of electric spark during the process of MAO and the quality of the coating on NiTi alloy surface. In this paper, it was studied systematically that the effects of additives on the morphology, composition and corrosion resistance of micro-arc oxidation coating by adding 0.03 mol/L NaOH, 0.03 mol/L NaH_2PO_2 and 0.03 mol/L Na_3PO_4 into the 0.2 mol/L NaAlO_2 electrolyte.

2. EXPERIMENTAL SECTION

2.1. Materials

NiTi alloy (Ni 50.8 at.%, Ti 49.2 at.%) with a diameter of 12 mm and a thickness of 3.5 mm was used as the substrate in this study. Before the MAO process, samples were ground with 320#, 600#, 800# and 1000# SiC abrasive papers, and next cleaned by ultra-sonic degreasing with pure ethanol and distilled water.

2.2. Preparation of MAO coatings

The MAO process was carried out with the equipment consisted of a bipolar pulsed DC power supply (constant voltage and constant current density modes are provided), a stainless steel cell, an air stirring system, and a cooling chamber system. In this study, the working mode adopted the constant voltage mode, and the voltage is 360 V. The frequency, duty cycle and processing time were 500 Hz, 45% and 30 min, respectively. Samples were used as anodes, a stainless steel cylinder container was used as the cathode. About 0.03 mol/L NaOH, NaH₂PO₂ and Na₃PO₄ as additives were respectively added to the basic electrolyte (sodium aluminate electrolyte of 0.2 mol/L). In order to distinguish different additives, the coatings after micro-arc oxidation were named as MAO-NaOH coating, MAO-NaH₂PO₂ coating and MAO-Na₃PO₄ coating, respectively. After the coating process, the MAO samples were cleaned with pure water and alcohol and then dried.

2.3. Surface Characterization

The scanning electron microscopy (SEM) equipped with energy-dispersive X-ray spectroscopy (EDS) analysis was used to observe the surface morphology. The phase composition of the MAO samples was investigated by X-ray diffractometer technology (XRD-7000S/L) using Cu-K α radiation at 40 kV and 30 mA with a scan range between 20° and 80° at a scanning speed of 2°/min.

Polarization test was performed using PARSTAT MC 2000 of a multi-channel multifunctional electrochemical workstation in simulated body fluid (SBF, composition was given in Table 1) at 37 °C. The three-electron system, including the coated sample as the working electrode, the platinum grid as the counter electrode, and a saturated calomel electrode (SCE) as the reference electrode, was used in the electrochemical experiments. In the potentiodynamic polarization tests, the working electrode was immersed in the SBF, and then polarized from the corrosion potential at a scanning rate of 0.5 mV/s. The sweep potential of potentiodynamic polarization curves was from -1 V to 1 V vs open circuit potential.

Table 1. The composition of simulated body fluid

Composition	Concentration (g/L)
NaCl	8.035
NaHCO ₃	0.355
KCl	0.225
K ₂ H ₂ PO ₄ ·3H ₂ O	0.231
MgCl ₂ ·6H ₂ O	0.311
CaCl ₂	0.292
Na ₂ SO ₄	0.072
Tris	6.118

Wear tests were performed using the MFT-R400 reciprocating wear testing machine at room temperature. To better simulate the wear behavior of micro-arc oxide ceramic coating in the human environment, this test was conducted in a simulated body fluid environment. As the counterpart, Si_3N_4 ceramic ball with a diameter of 5.5 mm was used. The parameters including the sliding speed (20 mm/s), sliding distance (12 m), the length of the wear track (5 mm), applying load (3 N) and sliding time (20 min) were chosen. After the friction and wear test, the samples were cleaned by ultrasonic using alcohol and deionized water in turn. The morphology of the worn track was observed by SEM. The contour of the cross-section of the worn track was measured by WIVS type white light interference three-dimensional profilometer.

3. RESULTS AND DISCUSSION

3.1. Morphology of the MAO coatings under different electrolytes

The surface morphologies of MAO coatings with different additives were shown in Fig. 1. Fig. 1a showed the surface morphology of MAO-NaOH coating. The surface of the MAO-NaOH coating was very rough, with a lot of white crystals covering the surface. There were no typical micro-arc oxidation discharge holes on the surface, and the number of micro-holes was small. The reason might be that the addition of NaOH led to the improvement of electrical conductivity, and the electric resistance of electrolyte was decreased. At the same time, strong micro-arcs would be generated effectively in higher voltages. Hence, the reaction speed was accelerated. Al_2O_3 produced in the process of MAO blocked reaction channels prematurely, resulting in an uneven reaction occurring on the surface. As the oxidation process continues, the reaction became difficult, and could be carried out partly. Thus the surface became rough and uneven.

Fig. 1b and c showed the surface morphology of the MAO- NaH_2PO_2 coating and MAO- Na_3PO_4 coating, respectively. It can be seen that the MAO- Na_3PO_4 coating was relatively rough, with poor flatness and microcracks. The MAO- NaH_2PO_2 coating presented a typical porous morphology with smooth surface and micropores. As shown in Fig. 1b, the size of the pores was not big enough to make a channel to permeate through the substrate for the corrosive media. Therefore, we preliminarily believed that the electrolyte system with NaH_2PO_2 additive was more favorable to the micro-arc oxidation of the NiTi alloy.

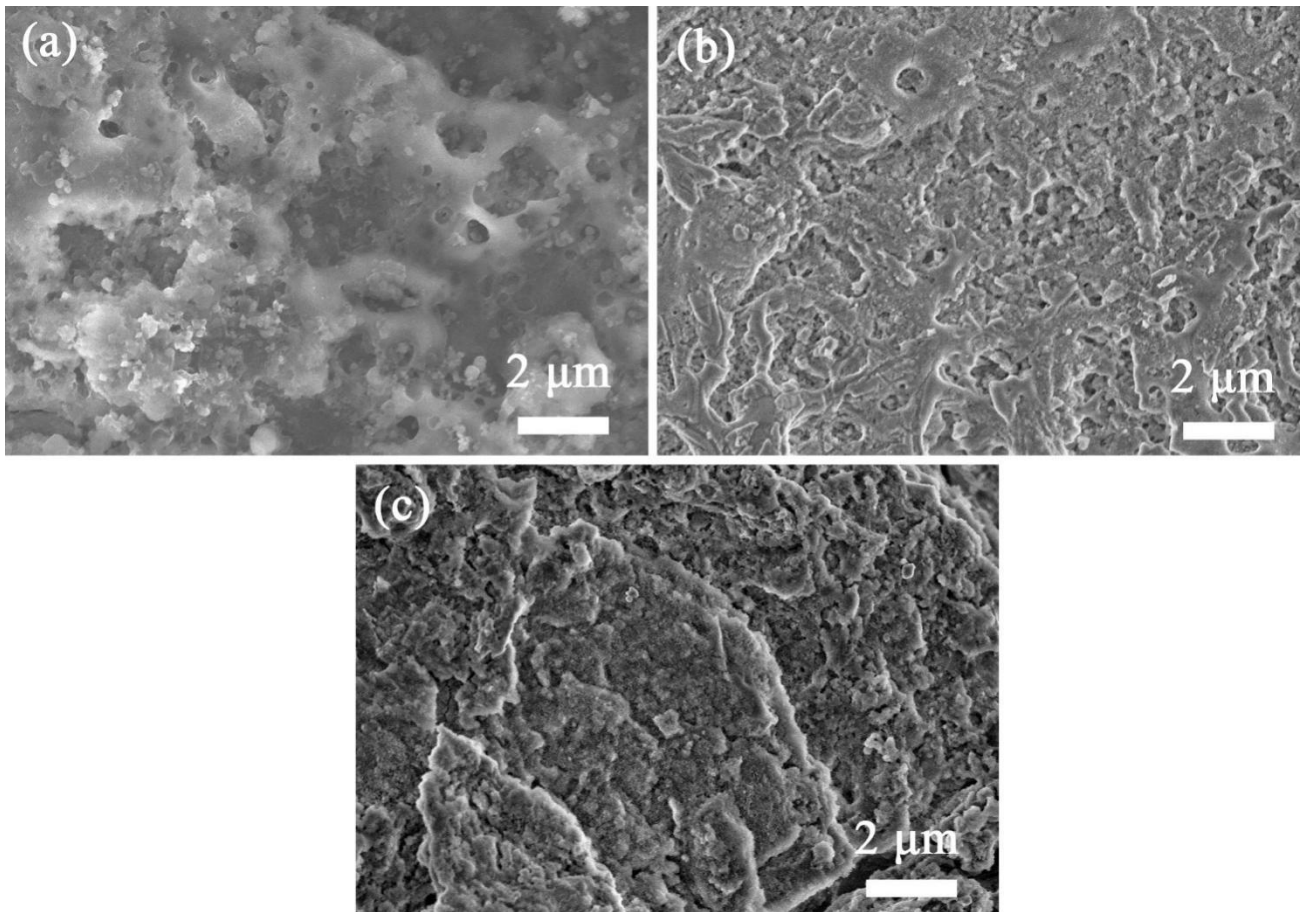


Figure 1. The SEM micrographs of the surface morphology of MAO coatings : (a) MAO-NaOH coating; (b) MAO-NaH₂PO₂ coating;(c)MAO-Na₃PO₄ coating

3.2 Corrosion resistance

Potentiodynamic polarization curves and corresponding results of (I) NiTi substrate, (II) MAO-NaOH coating, (III) MAO-NaH₂PO₂ coating, and (IV) MAO-Na₃PO₄ coating in SBF solutions were shown in Figure 2 and Table 2. Generally, MAO coatings exhibited a higher E_{corr} and a more negative i_{corr} , which indicated that the corrosion resistance was significantly improved[25]. According to the results(Fig. 2; Table 2), both the self-corrosion current density and self-corrosion potential moved in a more negative direction. On the other hand, it had been declared by Dehghanghadikolaei et al.[20] that the self-corrosion potential was usually less important compared with the self-corrosion current density. Galvele[26] also reported that the corrosion current intensity might present much more information about the electrochemical behavior of the material. The lower corrosion current density showed the coating undergoes less ion exchange during the corrosion process, indicating that the corrosion resistance had been improved. MAO-NaOH coating exhibited a more negative i_{corr} compared to the NiTi substrate, which indicated the corrosion resistance was significantly improved. Similar results were obtained with MAO-Na₃PO₄ coating and MAO-NaH₂PO₂ coating, respectively. By comparing the corrosion properties of the ceramic coating prepared by three additives, it was found that the corrosion current density of MAO-NaH₂PO₂ coating was the smallest, which was two orders of

magnitude lower than that of the NiTi substrate, indicating the corrosion resistance was the best. By observing the polarization curve of the MAO- NaH_2PO_2 coating, it could be found that the anode area had obvious passivation behavior, indicating that the coating inhibited the dissolution reaction. According to the discussion above, it could be obtained that the MAO- NaH_2PO_2 coating had better corrosion resistance.

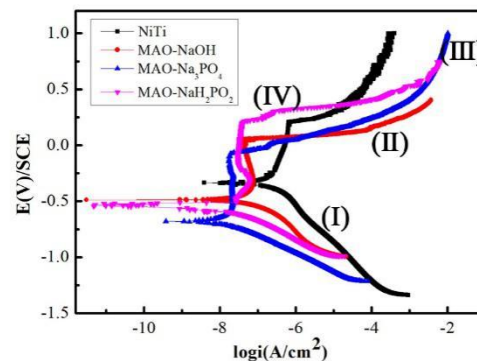


Figure 2. Potentiodynamic polarization curves of (I) NiTi substrate, (II) MAO-NaOH coating, (III) MAO- Na_3PO_4 coating, (IV) MAO- NaH_2PO_2 coating in SBF solutions.

Table 2. Electrochemical parameters of the polarization curves through Tafel fitting.

Sample	E_{corr} (mV)	i_{corr} (A/cm ²)
NiTi	-337	7.4×10^{-7}
MAO-NaOH	-496	4.2×10^{-7}
MAO- Na_3PO_4	-683	3.7×10^{-8}
MAO- NaH_2PO_2	-551	8.7×10^{-9}

3.3 Characterization of the MAO- NaH_2PO_2 coating

3.3.1 The cross-sectional morphology and composition distribution of the cross-section

According to the result of the electrochemical experiments, the MAO- NaH_2PO_2 coating had the best properties, thus it was mainly characterized as follows. Fig. 3 showed cross-section morphology of the MAO- NaH_2PO_2 coating and the corresponding EDS spectrum. It could be seen that the coating was composed of the dense inner layer and the loose outer layer, with an uneven surface and a lot of white crystals. The reason for the dense layer was that the electrochemical cell had met a sufficient potential difference, and with a breakdown of the electrolyte resistance generated sufficient discharged energy to the substrate[20]. However, with the thickening of the coating layer and the solidified fused alumina closing the discharge channel, breakdown became difficult, and the working voltage could not continue to increase. At the same time, arcs went out, and the coating became loose. The coating thickness was about 5.4 μm , and a significant separation was not observed between the coating and the sample. It showed that adhesive strength between the coating and the NiTi substrate was firmly good. The white crystals were considered to be Al_2O_3 , which could be confirmed in the subsequent XRD

spectrum. Fig. 3b showed the results of the corresponding line spectrum analysis. The elements of the coating were mainly Al, P, Ni, Ti, and O. Ni and Ti existed due to the base alloy composition, and Al and P existed due to the electrolyte used in the coating process. The existence of O was due to the strong affinity of Al for O, and thus Al_2O_3 formed quickly. Among them, the content of O and Al in the coating were high, while the content of Ni, Ti, and P was low, which was consistent with the XRD pattern. Compared with the substrate, the content of Ni in the MAO coating was much lower, which proved that micro-arc oxidation treatment could effectively reduce the content of Ni.

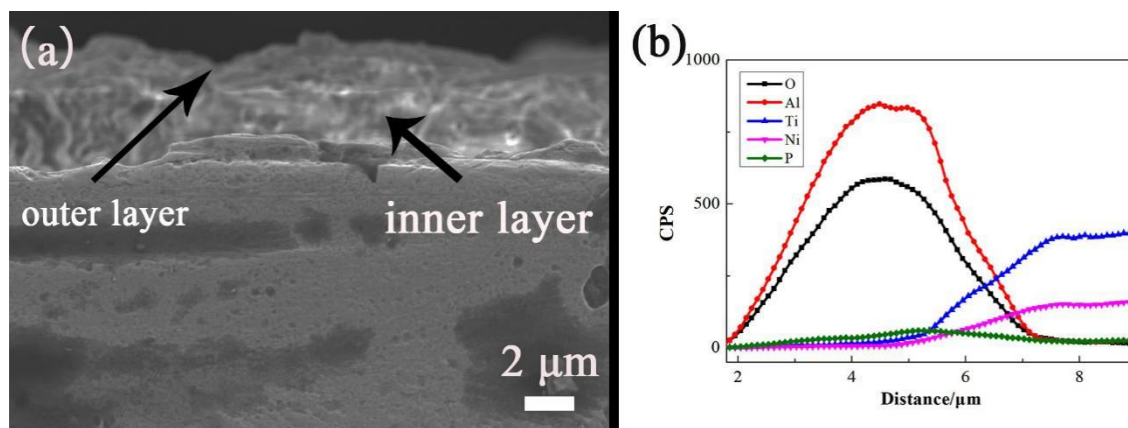


Figure 3. (a) A section morphology of the MAO- NaH_2PO_2 coating and (b) the corresponding EDS spectrum

3.3.2 The phase composition

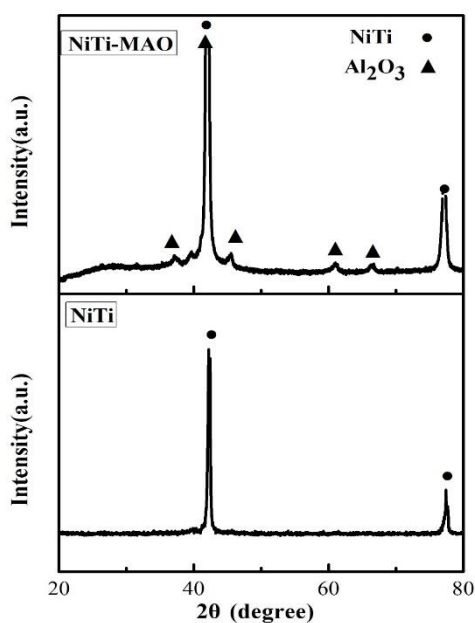


Figure 4. XRD pattern of the MAO- NaH_2PO_2 coating and untreated NiTi alloy

XRD patterns of the MAO- NaH_2PO_2 coating and untreated NiTi substrate were shown in Fig. 4. Compared with the substrate, Al_2O_3 phase was mainly observed in the coating, which was consistent with EDS results (Fig.3). The NiTi phase of the coating detected by XRD was from the substrate, because the MAO coating was so thin that the X-ray can penetrate it. The formation of Al_2O_3 phase is due to the decomposition reaction of $[\text{Al}_2\text{O}(\text{OH})_6]^{2-}$ (as shown in the following reaction) which exists in the NaAlO_2 solution[23].



3.3.3 Wear properties of MAO- NaH_2PO_2 coating

Friction coefficient curves of MAO- NaH_2PO_2 coating and the NiTi substrate in SBF solutions recorded during wear tests were shown in Fig. 5. The average friction coefficient of the NiTi alloy was 0.4. In the initial stage of friction, the friction coefficient fluctuated greatly, which was due to the rough surface composed of a large number of micro-convex peaks. In the initial stage, the friction pair started to contact with the micro-convex peaks, but the contact area was small, resulting in unstable friction process. As the friction continued, the contact area between the friction pair and the surface increased, resulting in a decrease in the friction coefficient. However, the friction coefficient of MAO- NaH_2PO_2 coating entered the stable friction stage after 2 minutes in SBF, and the friction coefficient remained unchanged at the value of about 0.7, which was significantly higher than that of the substrate. It was mainly due to the increase of surface roughness after micro-arc oxidation.

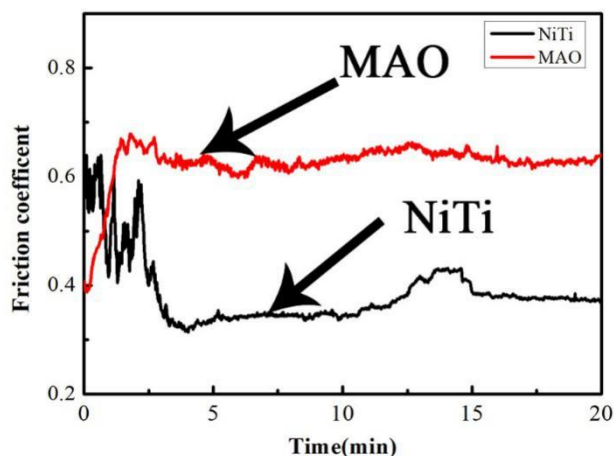


Figure 5. Friction coefficient of the MAO- NaH_2PO_2 coating and untreated NiTi alloy in SBF.

Fig. 6 showed the morphologies of the worn surface of NiTi alloy and MAO- NaH_2PO_2 samples. It could be seen that the worn surface morphology showed deep and wide grooves which were the typical wear characteristics of abrasive wear. There were many particles on the surface of worn tracks of NiTi alloy. Since the hardness of the NiTi alloy was lower than that of Si_3N_4 ceramic ball, the surface of the Si_3N_4 ceramic ball had a ploughing effect on NiTi alloy's surface, resulting in a large number of abrasive particles on NiTi alloy's surface. If the abrasive particles were not carried away by

the solution in time, they would directly participate in the friction process as abrasive particles, which further aggravated the wear of NiTi alloy. Therefore, the wear mechanism of NiTi alloy was mainly abrasive wear. In addition to the same abrasive wear characteristics were observed on the surface of MAO- NaH_2PO_2 coating, the MAO- NaH_2PO_2 coating also had slight adhesive wear. By comparing with NiTi substrate, it was found that the micro-arc oxidation specimens had a narrower width of worn tracks and better wear resistance. Table 2 showed the element composition of the MAO- NaH_2PO_2 coating worn surface. The results showed that the content of the element Al and element P on the MAO- NaH_2PO_2 worn surface was almost zero, indicating that the ceramic coating had been basically worn through after 20 minutes in the solution medium.

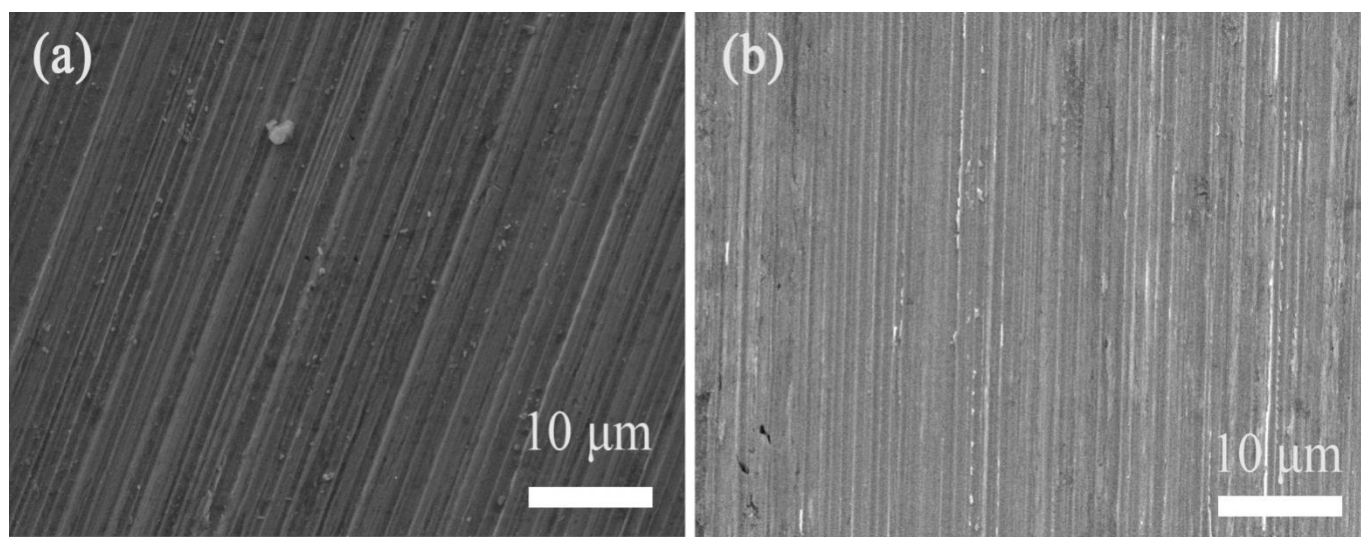


Figure 6. The worn surface morphology of the MAO- NaH_2PO_2 coating and untreated NiTi alloy in SBF

Table 2. Results of the element composition of the worn surface of the MAO- NaH_2PO_2 coating and untreated NiTi alloy in SBF

Element	Ni at.%	Ti at.%	Al at.%	O at.%	P at.%
NiTi	47.0	44.9	0	7.8	0
MAO	47.2	45.9	0.2	6.6	0.1

Fig.7 showed the wear profile curves of the NiTi substrate and MAO- NaH_2PO_2 coating. The depth and width of the worn tracks could be determined by the 2-D worn track profiles. Thus the volume of wear tracks and wear rate could be calculated. The wear parameters obtained by calculation of the substrate and the MAO- NaH_2PO_2 coating were presented in Table 3. The width of the MAO- NaH_2PO_2 coating was 0.3 mm, which was significantly lower than that of the substrate, which was 0.6 mm. The depth of the MAO- NaH_2PO_2 coating was 5.4 μm , while the depth of the substrate was 13.0 μm , indicating that the coating was indeed worn through during the friction process, which was also confirmed by EDS results of the worn crack. By comparing the wear volume, it was found that the wear volume of the micro-arc oxidation sample under the optimal process was $5.4 \times 10^{-3} \text{ mm}^3$, which

was 77.5% lower than that of $2.4 \times 10^{-2} \text{ mm}^3$ of the substrate, indicating that the wear resistance of the NiTi alloy could be significantly improved after the MAO treatment. The increased wear resistance may be due to the formation of Al_2O_3 on the surface.

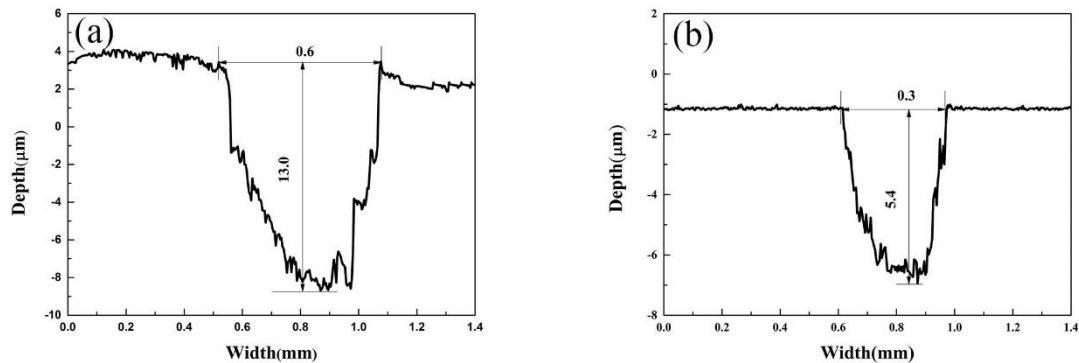


Figure 7. The wear profile curves of the MAO- NaH_2PO_2 coating and untreated NiTi alloy in SBF

Table 3. Results of the wear parameters of the MAO- NaH_2PO_2 coating and untreated NiTi alloy in SBF

Sample	b/mm	h/ μm	Wv/ mm^3	K/ $\text{mm}^3 \cdot \text{N}^{-1} \cdot \text{m}^{-1}$
NiTi	0.6	13.0	2.6×10^{-2}	6.7×10^{-4}
NiTi-MAO	0.3	5.4	5.4×10^{-3}	1.5×10^{-4}

4. CONCLUSION

In this study, corrosion resistance of MAO coatings fabricated on the NiTi alloy in sodium aluminate base electrolyte with three different additions of NaOH, Na_3PO_4 and NaH_2PO_2 were studied. The optimum electrolyte system was determined and characterized.

1. The ceramic coating was fabricated on the surface of the NiTi alloy by micro-arc oxidation technology. The optimal coating (MAO- NaH_2PO_2 coating) was determined by studying the surface morphology and the corrosion resistance of the coating with different additives.

2. The uniform MAO- NaH_2PO_2 ceramic coating with the thickness of 5.4 μm was prepared, which mainly composed of Al_2O_3 .

3. The wear performance of the MAO- NaH_2PO_2 coating was studied. The wear mechanism of the NiTi substrate and MAO- NaH_2PO_2 coating were abrasive wear. The wear volume of micro-arc oxidation coating was 77.5 % lower than that of the substrate, which showed that the micro-arc oxidation treatment could significantly improve its wear resistance.

ACKNOWLEDGMENTS

This work was supported by the Natural Science Foundation of Shanxi Province (No. 201901D111063)

Reference

1. R.Q. Hang, Y.L. Liu, L. Bai, M. Zong, M.X. Zong, X. Wang, X.Y. Zhang, X.B. Huang, B. Tang, *Materials Letters*, 202 (2017) 5.
2. 2.C.F. Dunne, K. Roche, B. Tworney, K.T. Stanton, Stanton Kenneth T, *Materials Letters*, 176(2016) 185.
3. D.G. Barceloux, D. Bareloux, *Journal of Toxicology: Clinical Toxicology*, 37(1999) 239
4. E. Denkhaus, K. Salnikow, *Critical Reviews in Oncology/ Hematology*, 42(2000) 35.
5. J.K. Bass, H. Fine, G.J. Cisneros, *American Journal of Orthodontics and Dentofacial Orthopedics*, 103(1993) 280.
6. C.L. Chu, R.M. Wang, L.H. Yin, Y.P. Pu, P.H. Lin, Y.S. Dong, C.Y. Chung, K.W.K. Yeung, P.K. Chu, *Materials Letters*, 62(2008) 3512.
7. A.R. Boccaccini, J. Cho, J.A. Roether, B.J.C. Thomas, E. Jane Minay, M.S.P. Shaffer, *Carbon* 44(2006) 3149.
8. M.R. Etminanfar, J. Khalil-Allafi, A. Montaseri, R. Vatankhah-Barenji, *Mater. Sci. Eng. C Mater. Biol. Appl.*, 62 (2016) 28.
9. F. Marashi-Najafi, J. Khalil-Allafi, M.R. Etminanfar, *Mater. Sci. Eng. C Mater. Biol. Appl.*, 76 (2017) 278.
10. K.W. Ng, H.C. Man, T.M. Yue, *Applied Surface Science*, 257(2011) 3269.
11. Z.D. Cui, H.C. Man, X.J. Yang, *Surface and Coatings Technology*, 192 (2005) 347.
12. B. Fu, K. Feng, Z. Li, *Materials Letters*, 220 (2018) 148.
13. Y. Cheng, Y.F. Zheng, *Materials Science and Engineering: A*, 434 (2006) 99.
14. A. Shanaghi, P.K. Chu, *Surface and Coatings Technology*, 365 (2019) 52.
15. J. Wang, N. Jiang, *Diamond and Related Materials*, 18 (2009) 1321.
16. R. Hang, S. Ma, P.K. Chu, *Diamond and Related Materials*, 19 (2010) 1230.
17. Z. Huan, L.E. Fratila-Apachitei, I. Apachitei, J. Duszczuk, *Applied Surface Science*, 258 (2012) 5244.
18. J.L. Xu, F. Liu, F.P. Wang, D.Z. Yu, L.C. Zhao, *Applied Surface Science*, 254 (2008) 6642.
19. L.O. Snizhko, A.L. Yerokhin, A. Pilkington, N.L. Gurevina, D.O. Misnyankin, A. Leyland, A. Matthews, *Electrochimica Acta*, 49 (2004) 2085.
20. A. Dehghanhadikolaei, H. Ibrahim, A. Amerinatanzi, M. Hashemi, N.S. Moghaddam, M. Elahinia, *Journal of Materials Science*, 54 (2019) 7333.
21. H.R. Wang, F. Liu, Y.P. Zhang, F.P. Wang, *Surface and Coatings Technology*, 206 (2012) 4054.
22. H.R. Wang, F. Liu, Y.P. Zhang, D.Z. Yu, F.P. Wang, *Applied Surface Science*, 257 (2011) 5576.
23. J.L. Xu, F. Liu, F.P. Wang, L.C. Zhao, *Materials Letters*, 62 (2008) 4112.
24. 24.K. Zhang, S.R. Yu, *Surface and Coatings Technology*, 388 (2020) 125453.
25. C.Y. Li, X.L. Feng, X.L. Fan, X.T. Yu, Z.Z. Yin, M.B. Kannan, X.B. Chen, S.K. Guan, J. Zhang, R.C. Zeng, *Advanced Engineering Materials*, 21 (2019) 1900446.
26. J.R. Galvele, G.S. Duffo, *Corrosion Science*, 39 (1997) 605